Rapid #: -19423109

CROSS REF ID: **975048**

LENDER: **UKROH :: Main Library**

BORROWER: **EYW :: Main Library**

TYPE:	Article CC:CCG
JOURNAL TITLE:	Fuel
USER JOURNAL TITLE:	Fuel
ARTICLE TITLE:	Effect of gas composition on the performance and emissions of a dual-fuel diesel-natural gas engine at low load conditions
ARTICLE AUTHOR:	Ulishney, Christopher
VOLUME:	324
ISSUE:	
MONTH:	
YEAR:	2022
PAGES:	124531-
ISSN:	0016-2361
OCLC #:	

Processed by RapidX: 8/22/2022 1:27:09 AM

Fuel 324 (2022) 124531

Contents lists available at ScienceDirect

Fuel

journal homepage: www.elsevier.com/locate/fuel

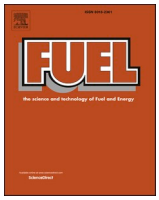

Full Length Article

Effect of gas composition on the performance and emissions of a dual-fuel diesel-natural gas engine at low load conditions

Christopher J. Ulishney, Cosmin E. Dumitrescu *

West Virginia University, Mechanical and Aerospace Engineering Department, Morgantown, WV 26506, USA

ARTICLE INFO

Keywords:
Natural gas
Dual fuel
Fuel effects
Gas composition effects

ABSTRACT

Areas located at or near natural gas (NG) well or storage sites can use NG to partially or totally replace the diesel fuel used to power equipment or for local transportation. This study investigated a dual-fuel diesel-NG engine operating at low load conditions, as literature shows that such conditions are the most sensitive to NG composition. Part of the diesel fuel was replaced with four different gas blends containing methane, ethane, and propane. No EGR was employed to avoid it interfering with the individual fuel component evaluation. Results show up to 80% higher rates of pressure rise compared to the diesel baseline, which limited the diesel substitution rate to 40% without EGR. While pure methane affected the most the diesel fuel vaporization and ignition delay, important differences were seen during the late-stage fuel oxidation. The location and magnitude of the 2nd heat release peak changed with gas composition, with propane gas mixtures showing the largest and most advanced peak. In-cylinder pressure correlated with the gas mixture' autoignition temperature. As a result, the mixtures with propane had the best performance and gaseous fuel oxidation, with opposite results for the methane-only gas. As propane gas mixtures performed better than mixtures with ethane, it suggests maintaining a higher propane fraction in the NG for dual-fuel operation. CO_2 and NO_x emissions reduced up to 6.8% and 20%, respectively. However, the reduction was offset by the large increase in CO and HC emissions, which could require after-treatment modifications. Finally, the results suggest that the switch from diesel only to low-load dual-fuel operation can be performed without major modifications in terms of engine control and aftertreatment changes, at least for the low load conditions and NG compositions used here.

1. Introduction

Strong demand and reduced refining activities are affecting the level of diesel supplies in the U.S. [1]. As almost all heavy-duty internal combustion (IC) engines used for power generation or transportation are running on diesel, this will translate into higher costs for the end user. A solution to mitigate the issue is to replace diesel with alternative fuels such as the increasingly available natural gas (NG), whenever this is feasible. For example, areas located at or near NG well or storage sites can use NG to partially or totally replace the diesel fuel used to power equipment or for local transportation. This can have climate benefits too, as the lower carbon-to-hydrogen ratio of NG compared to diesel can reduce greenhouse gas emissions [2]. However, diesel conversion technologies were generally developed to use pipeline NG; therefore, changes in the local supply relative to the pipeline NG composition can be an issue for the IC engine operation. Specifically, pipeline NG is primarily composed of methane (CH_4 or C_1 in this study), with variable amounts of other naturally occurring hydrocarbons (HC) such as ethane (C_2H_6 or C_2 in this study) or propane (C_3H_8 or C_3 in this study), plus carbon-dioxide (CO_2), nitrogen (N_2), etc. [3]. But the well site NG can contain higher C_2-C_3 amounts plus other natural gas liquids (NGL) components such as butane (C_4H_{10} or C_4) and pentane (C_5H_{12} or C_5), which are usually allowed only in limited amounts in the pipeline NG. The reason is that it is more valuable to use the C_2-C_5 components to produce other chemicals of interest, hence they are typically separated from the pipeline NG. But NGL storage space can become an issue when the C_2-C_5 demand is low and, as a result, gas companies can be forced to flare the excess C_2-C_5. A solution is to increase the utilization of C_1-C_5 components as replacement for the diesel fuel used at the NG well or storage site or for local transportation. This would save on diesel fuel costs as well on the wasted energy during flaring. But the diesel engine modification cost is also important. The literature shows that a high diesel replacement fraction generally requires major engine work (e.g., new pistons, new ignition strategies, major aftertreatment changes, etc.)

* Corresponding author.
E-mail address: cedumitrescu@mail.wvu.edu (C.E. Dumitrescu).

https://doi.org/10.1016/j.fuel.2022.124531
Received 25 February 2022; Received in revised form 30 April 2022; Accepted 4 May 2022
Available online 10 May 2022

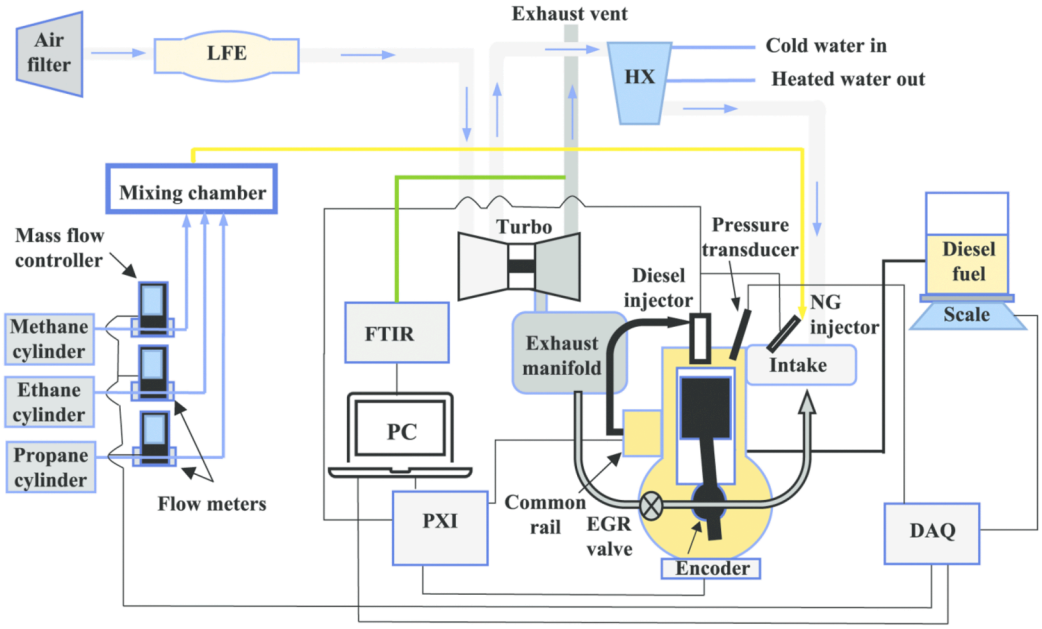

Fig. 1. Schematic of the engine experimental setup.

[4 5], which can be expensive. However, a lower diesel replacement fraction or a higher diesel replacement fraction done at lower engine load would not require the major engine modifications mentioned above. Therefore, the economic benefit is maintained [6].

This study was based on the hypothesis that with minimal processing (i.e., just enough to eliminate components that may damage the engine, such as hydrogen sulfide) the raw NG at the production or storage site can be safely utilized as replacement for the diesel fuel. Specifically, the original diesel engine can be modified to operate as dual-fuel engine without major effect on its efficiency, maintenance costs, and lifespan. As C_1-C_3 are the major hydrocarbons in NG (i.e., they have the largest percentage in the blend by volume), the following literature review discusses only their effect on engine performance. Variable C_1-C_3 percentage will affect NG's physical and chemical properties such as density, viscosity, low heating value (LHV), and flame speed, therefore yielding different combustion characteristics [7]. A larger C_2 or C_3 percentage will increase NG's energy content by volume, therefore a higher engine power for the same gas flow [8]. In addition, NG composition influences the chemical reaction rates, which affects the rate at which the pressure and temperature change inside the combustion chamber. This will affect the combustion phasing, duration, and completeness, therefore engine efficiency and emissions [9]. For example, C_1, the primary component of NG, has a higher autoignition temperature than C_2 or C_3 ($C_3 < C_2 < C_1$) [10 11], which means that it would be easier to control C_1 combustion timing in a dual-fuel NG-diesel engine compared to C_2 or C_3, as it is the diesel fuel that initiates the combustion process. Then, C_3 has the highest laminar flame speed (S_L), followed by C_2 and C_1, which suggests that a larger C_3 fraction will make the NG burn faster and more completely [7]. But engine performance sensitivity to C_1-C_3 percentage was shown to be dependent on engine load and speed. Specifically, combustion characteristics of dual-fuel diesel-NG engines deteriorate at lower load conditions [12]. For example, a higher methane content decreases the thermal efficiency [13] due to a lower peak pressure and higher ignition delay compared to the baseline diesel [14]. A small increase in thermal efficiency was noticeable in natural gas mixtures with lower methane content at higher fuel energy substitution rates, but less noticeable at levels below 40% energy substitution [13]. Numerical simulations suggested that increasing the methane percentage will influence the ignition delay by changing the specific heat of the mixture, in addition to the mixture dilution effect [15]. Both effects reduced chemical reactivity during the low temperature combustion phase but increase the global reactivity and temperature [15]. The combustion heat release rate occurs faster than traditional diesel when using 80% NG substitution rate [16]. However, the suggested maximum NG substitution rates at lower engine load was 40–45% of the total energy due to unacceptable methane emissions [17]. This was due to the very low NG equivalence ratio (ϕ) at low load (ϕ = 0.2–0.25); therefore, the primary flame initialization occurs and is sustained via the autoignition of diesel [18]. This was confirmed by optical studies, which showed that the flame kernel formation was scattered throughout the combustion chamber at 70%-85% NG energy substitution rates [19]. So, the differences in laminar flame speed between the C_1-C_3 components may not be as important under these extra-lean in-cylinder conditions that are experiencing volumetric ignition. Another issue at low load and high substitution rates is that the diesel amount can become smaller than what typical injectors were designed to deliver, making injections unstable and with less chance of igniting the natural gas mixture [20]. A solution for this extreme case is to shift to a two-stage autoignition combustion mode by greatly advancing the diesel injection timing to values that are mainly determined mainly by the mixture temperature [21]. All the above help explain the poor C_1-C_3 oxidation and high carbon monoxide (CO) concentrations in the exhaust at low load conditions.

The goal in this study was to perform a systematic evaluation of the effect of the C_1-C_3 percentage on the performance and emissions of a diesel engine operated in a NG-diesel dual-fuel mode, at low load conditions. The engine used in this work was representative of medium-duty turbo-charged diesel engines used for power generation at NG well or storage sites. While EGR would allow for increased diesel replacement fractions, it was not used here. The total NG + diesel fuel energy was constant for all C_1-C_3 blends, so any changes in the combustion characteristics could be directly attributed to the change in the blend's physical and chemical properties. The diesel injection timing was changed in steps small enough to not affect the efficiency but large enough to produce significant differences in combustion behavior and emissions. Engine speed and load were kept constant at values that authors want to use for future dual-fuel investigations in a similar engine but with extensive optical access (i.e., experiments were run at an engine speed and load that would not damage the optical engine but be representative for investigating gaseous fuel effects in a dual-fuel

Table 1
Engine specifications.

Engine Type	4-cylinder, 4-stroke Diesel, Turbocharged, Common Rail
Engine Make and Model	John Deere 4045-HFC04
Bore and Stroke [mm]	106×127
Displacement [L]	4.5
Compression Ratio	17.0:1
Fuel System Diesel/NG	Direct Injection/Sequential Port Fuel Injection
Piston Shape	Bowl-in piston
IVO/IVC [CAD]*	338.7/570
EVO/EVC [CAD]*	138.25/361.8
Low Idle Speed	800 RPM
Rated Power/Speed	93–129 kW at 2200–2400 RPM

* 0 CAD is the TDC compression/firing.

operation). As a result, the objective was to determine the maximum diesel replacement fraction before significant changes were observed in terms of efficiency, emissions, and possible engine structural damage, and how the C_1-C_3 percentage affected this change. Suggestions about how to address observed issues in terms of engine control were also presented. The Wobbe Index (WI), methane number (MN), and Propane Knock Index (PKI) of each blend were also provided to make it easier to compare the results with existing literature.

2. Experimental setup

The engine used in this study was a 4-cylinder, 4.5-L Tier 4 turbocharged industrial diesel engine (John Deere, Model 4045-HFC04), converted to dual-fuel operation with the addition of four NG low-pressure injectors (Rail Spa, Model IG7 Navajo) that delivered NG just above the intake valve location. Fig. 1 shows a schematic of the engine experimental setup and Table 1 lists engine specifications.

As engine control software is proprietary, commercially available hardware and software were adapted or modified to allow for the total control of engine operating parameters and the transition to dual-fuel operation. For example, commercial software (National Instruments (NI) LabVIEW and DRIVVEN CalVIEW) and hardware (NI PXI 8106) alongside various engine control cards such as Drivven Direct Injector drivers, Drivven Port Fuel Injector drivers, Drivven AD-Combo, Drivven Low-Side controller, and NI-9401 and NI-9402 expansion cards controlled the diesel and/or gas pressure, injection duration, and timing, the EGR and boost valve, etc. The software was also modified to output to the data acquisition system (DAQ) several other signals of interest for data analysis such as the diesel injection command and duration, the encoder Z-pulse, etc.

A separate system, also based on NI software, controlled and collected the dynamometer (Medsker Electric Inc.) speed and torque, the gas flow rates (AliCat MCP-series for C_1 and MC-series for C_2 and C_3), the pressure relief valve for the diesel common rail, and other low-frequency engine data such as thermocouples (for intake air, coolant, oil, gas, exhaust, etc.), the digital scale (Brecknell MBS-6000) used to quantify the diesel fuel consumption, the EGR valve position, etc. Air flow was measured using a 4-inch laminar flow element (LFE; Meriam Model Z50MC2-4) with classical coefficients and then standardized within the LabVIEW program. Air flow was corrected for ambient humidity. A heat exchanger (HX) was placed on the air intake line to control the air temperature after the turbo. A pressure transducer (Kistler 6056A), mounted via a glow plug adapter (Kistler 6542Q) and connected to a charge amplifier (Kistler 5010B) measured in-cylinder pressure data, which was then transferred via a National Instruments SCB-68A fast data acquisition board to another LabVIEW-based data acquisition system that recorded it. The SCB-68A also collected high-speed data from the engine encoder, the high-frequency intake and exhaust pressure sensors, and the injection command signal. The high-frequency pressure data was used to peg in-cylinder pressure data to the intake and exhaust pressure at the time of intake valve closing or exhaust valve opening, respectively.

An FTIR gas analyzer (MKS, Model Multigas 2030, controlled via MKS MG2000 software) measured engine out emissions. The emission analyzer was verified with two certified blends prior to the start of data collection. A heated line (Atmo-Seal, Model IGH, 190 °C) delivered sample emissions to the gas analyzer for measurements.

Table 2 details the composition and properties of the fuel blends investigated in this work. The fuel blends are described here by their name following a notation of M for C_1, E for C_2, and P for C_3, then followed by the molar (volumetric) percentage of each fuel in the gas blend. For example, M90E10 represents a blend with 90% by volume methane and 10% by volume ethane. It should be mentioned that the GRI MECH III – based laminar flame speed at atmospheric conditions [22] shown in Table 3 varies inversely with the LHV, WI, and MN of the fuel blend but varies directly with the molecular weight (MW), density, and PKI of the gas blend.

The experiments were performed under steady state low load (~25% maximum rated brake mean effective pressure (BMEP)) conditions at 1000 RPM and three different diesel injection timings (SOI_{DIESEL}), −8 CAD ATDC, −4 CAD ATDC, and 0 CAD ATDC (or TDC). The diesel injection timings selected were centered about the baseline diesel maximum brake torque (MBT) timing of −4 CAD ATDC. The relatively limited SOI_{DIESEL} range was due to the unacceptable rates of pressure rise for SOI_{DIESEL} earlier than –8 CAD ATDC and the unacceptable HC and CO emissions for SOI_{DIESEL} later than TDC. The diesel condition was repeated three times with each dual-fuel case repeated twice, and mean values and standard deviations of the measurements are presented. The diesel fuel injection pressure and substitution rate were maintained constant at 1000 bar and 40%, respectively. The diesel replacement fraction was limited by the desire to avoid the use of EGR (i.e., to minimize the rate of in-cylinder pressure rise) and to a value that, for real applications, can maintain the original OEM ECU diesel system control. Subsequently, a greater CO_2 reduction in addition to the fuel cost and availability benefit was not the primary focus here. The fueling conditions resulted in a 25% decrease of the diesel injection duration from 4.8 CAD for diesel only operation to 3.6 CAD for the dual-fuel operation. Eq. (1) shows the diesel substitution formula, where $\dot{E}_{Diesel}$ and $\dot{E}_{NG}$, are the diesel and C_1-C_3 blend energy content per unit time, respectively:

$$(Diesel)\ Substitution\ Rate = \frac{\dot{E}_{NG}}{\dot{E}_{Diesel} + \dot{E}_{NG}} \quad (1)$$

Experimental data was post-processed using MATLAB©. Emissions data was stabilized between test runs then collected over several minutes of steady-state engine operation. Average emission calculations were performed using a graphical user interface program based on CFR part 1065. Nitrogen dioxide and nitric oxide emissions were combined

Table 2
Selected properties of C_1-C_3 gas mixtures.

Mixture Name	MW [kg/kmol]	LHV [kJ/kg]	AFR Mass	Density [kg/m^3]	Wobbe Index [kJ/kg]	MN [23]	PKI [23]	S_L* [cm/s]
M100	16.04	50,000	17.12	0.668	74,582	100	0	38.22
M90E5P5	18.14	49,374	16.83	0.759	68,819	72	6.1	39.87
M90E10	17.44	49,621	16.92	0.728	70,657	81	2.9	38.82
M90P10	18.85	49,146	16.75	0.789	67,110	66	10	41.05

* For a stoichiometric mixture at 300 K and 1 atm (GRI MECH III).

Table 3
Average and standard deviation of global equivalence ratio, BMEP, brake efficiency, BSFC, and COV_{IMEP}, as function of the fuel composition and the diesel start of injection.

SOI (CAD ATDC)	Fuel type	Global ϕ [-]	BMEP [bar]	Brake Efficiency [%]	BSFC [g/kwh]	COV of IMEP [%]
−8	Diesel	0.55 +/- 0.03	6.55 +/- 0.23	39.1 +/- 1.3	215 +/- 7	3.59
	M100	0.54 +/- 0.03	6.09 +/- 0.27	35.9 +/- 1.5	222 +/- 9	2.41
	M90E5P5	0.52 +/- 0.03	6.07 +/- 0.30	36.2 +/- 1.7	221 +/- 10	2.47
	M90E10	0.54 +/- 0.04	6.11 +/- 0.29	35.7 +/- 1.6	224 +/- 10	2.57
	M90P10	0.54 +/- 0.04	6.18 +/- 0.30	36.5 +/- 1.7	219 +/- 10	2.55
−4	Diesel	0.55 +/- 0.03	6.71 +/- 0.23	39.5 +/- 1.3	214 +/- 7	3.51
	M100	0.54 +/- 0.03	6.13 +/- 0.31	36.2 +/- 1.7	220 +/- 10	2.47
	M90E5P5	0.52 +/- 0.03	6.14 +/- 0.28	36.5 +/- 1.6	219 +/- 10	2.61
	M90E10	0.53 +/- 0.04	6.16 +/- 0.29	35.9 +/- 1.6	223 +/- 10	2.71
	M90P10	0.53 +/- 0.04	6.24 +/- 0.29	36.9 +/- 1.6	217 +/- 10	2.64
0	Diesel	0.54 +/- 0.03	6.59 +/- 0.22	39.1 +/- 1.3	213 +/- 7	3.73
	M100	0.53 +/- 0.03	6.06 +/- 0.28	35.8 +/- 1.6	223 +/- 10	2.54
	M90E5P5	0.52 +/- 0.03	6.07 +/- 0.28	36.0 +/- 1.6	222 +/- 10	2.59
	M90E10	0.53 +/- 0.03	6.04 +/- 0.27	35.1 +/- 1.5	227 +/- 10	2.64
	M90P10	0.53 +/- 0.03	6.21 +/- 0.29	36.6 +/- 1.6	219 +/- 10	2.67

during post processing to produce a single NO_x value. The specific emission values were calculated with respect to brake power.

3. Results and discussion

This section presents and discusses the dual-fuel engine performance and emissions compared to diesel-only operation (or baseline diesel). A minimum of 200 cycles under the investigated operating condition were collected and used for analysis. The intake temperature was maintained at 35 °C ± 5 °C, intake pressure was 1.17 bar ± 0.02 bar, and premixed fuel equivalence ratio was 0.21–0.22 for all tests. First, Table 3 is presented. It shows the change in the global mixture equivalence ratio (i.e., diesel plus gas) and brake specific fuel consumption (BSFC). Table 3 also shows the expected decrease in BMEP and brake thermal efficiency when 40% of the diesel was replaced with the C_1-C_3 blend; the magnitude and origin of these decreases will be discussed later in the narrative. The coefficient of variation of the indicated mean effective pressure (COV_{IMEP}) lower than 4% shows that the dual-fuel mode did not degrade combustion stability at this substitution rate and lower load operation.

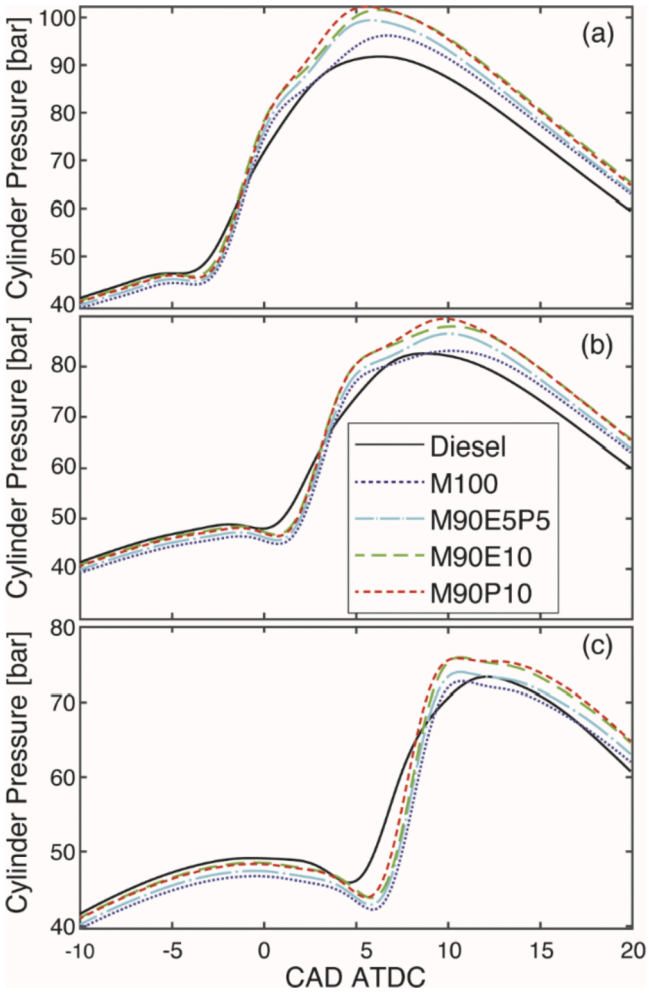

Fig. 2. Effect of fuel composition on in-cylinder pressure at (a) SOI_{DIESEL} = –8 CA ATDC, (b) SOI_{DIESEL} = −4 CA ATDC, and (c) at SOI_{DIESEL} = TDC.

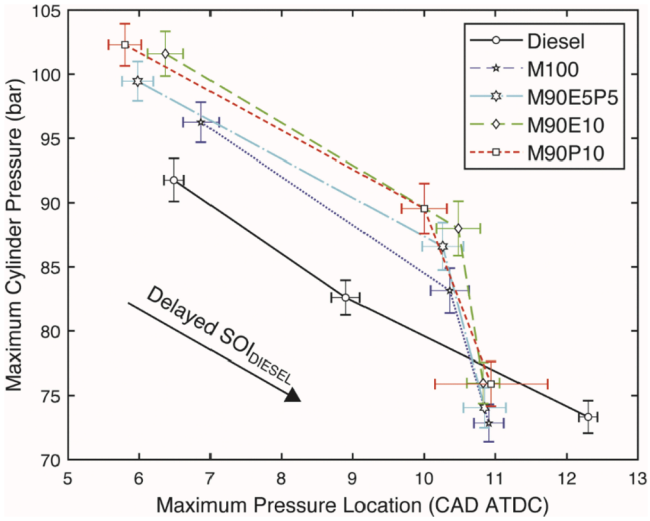

Fig. 3. Influence of fuel composition and SOI_{Diesel} on the magnitude and location of the maximum in-cylinder pressure. Error bars represent their cycle-to-cycle standard deviation.

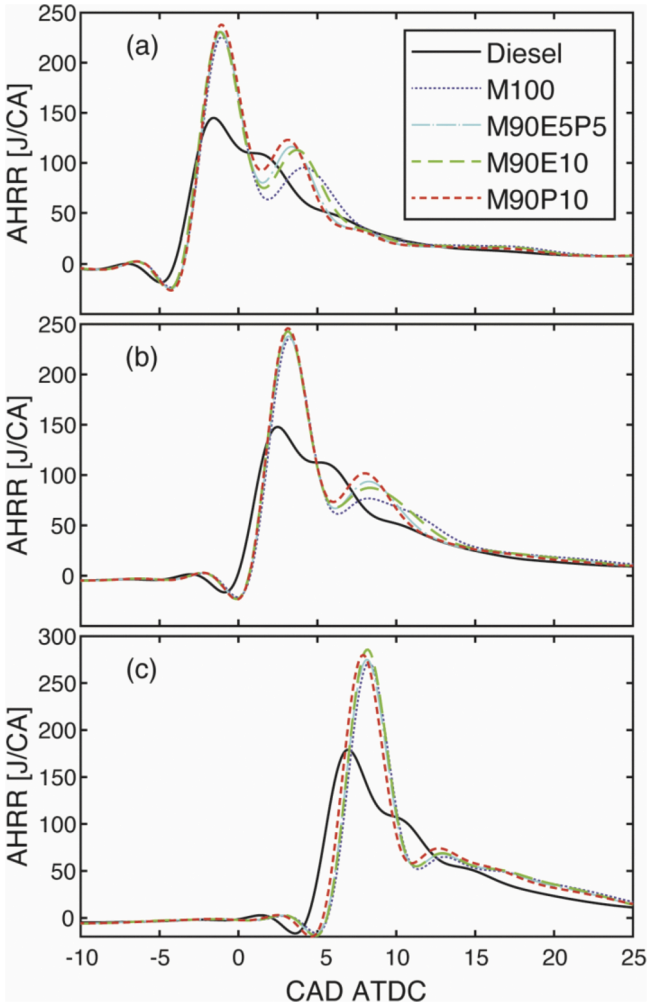

Fig. 4. Apparent heat release rate at several diesel injection injections timings: (a) at SOI_{DIESEL} = –8 CA ATDC, (b) at SOI_{DIESEL} = −4 CA ATDC, and (c) at SOI_{DIESEL} = TDC.

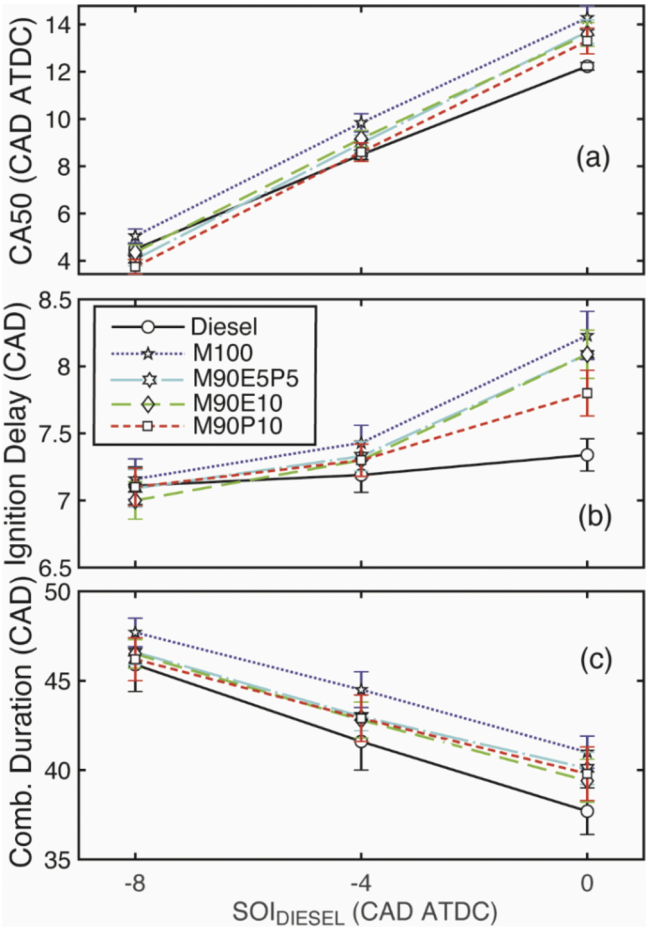

Fig. 5. Effect of C_1-C_3 composition on combustion phasing: (a) effect on CA50, (b) effect on the ignition delay, and (c) effect on the combustion duration. Error bars represent their cycle-to-cycle standard deviation.

The data in Table 3 was presented to aid with in-cylinder pressure data analysis and the associated discussions, which are presented next.

The Introduction section mentioned that the addition of the gaseous fuel increases the ignition delay under dual-fuel operation relative to baseline diesel operation. Fig. 2 suggests that the longer ignition delay was the result of a delayed diesel vaporization compared to baseline diesel operation. While the effect is seen for all gas blend compositions, the actual C_1-C_3 percentage influenced the magnitude of the delay. M100 increased the delay the most, while M90P10 and M90E10 had a lesser effect. The shortest delay in diesel fuel vaporization shifted from M90E10 at SOI_{DIESEL} = −8 CAD ATDC to M90P10 at SOI_{DIESEL} = TDC, with a near equal ignition delay at SOI = −4 CAD ATDC. A closer inspection of in-cylinder pressure traces shows that the delay correlated with the up to 3 bar decrease in pressure just before the start of the diesel injection, with M100 showing the lowest in-cylinder pressure at SOI_{DIESEL}. As the differences in intake pressure and temperature between the baseline diesel and the dual-fuel operation mentioned previously are not enough to completely explain the decrease in pressure just before the start of the diesel injection, the data suggests that the increase in vaporization delay was due to the changes in the specific heat of the mixture. A different specific heat will change the polytropic coefficient, hence the change in the temperature and pressure at the end of the compression stroke. This supports the simulation findings in ref. [15]. Then, the actual SOI_{DIESEL} affected the vaporization delay magnitude, with the delay increasing from 1 CAD at SOI_{DIESEL} = − 8 CAD ATDC to 2 CAD at SOI_{DIESEL} = TDC. The additional timing allowed the diesel fuel to penetrate even further inside the combustion chamber, therefore a better air-diesel mixing before ignition. This explains why, even if the combustion process started later than for the baseline diesel case, the pressure increased faster in the dual-fuel mode. Specifically, the maximum rate of pressure rise increased from 7 to 8 bar/CAD for diesel to 12–14 bar/CAD for the dual-fuel cases, or an almost 80% increase. The lengthened ignition delay results in a more rapid and intense heat release [24]. This substantial increase in the rate of pressure rise is important when considering its effect on the structural integrity of the engine. It also supports the maximum substitution rate of 40–45% mentioned in ref. [17] but, if just the rate of pressure rise is a concern, there are ways to mitigate it, such as the use of EGR to slow the combustion. The substantial increase in the pressure rise at this low load operating condition is also attributed to the high turbulence inside the bowl region of the piston near TDC [25 26], which further accelerates the premixed combustion process (i.e., fast burn). However, the almost parallel pressure lines throughout the fast burn period seen in Fig. 2 for each respective fuel suggests that SOI_{DIESEL} did not have a large influence on the rate of pressure rise, for both baseline diesel and dual-fuel operation. With regards to the actual C_1-C_3 percentage effect; M90P10 had consistently the highest maximum in-cylinder pressure, followed by M90E10, M90E5P5, and M100, which is correlated with the auto-ignition temperature ranking mentioned in the Introduction section.

The maximum in-cylinder pressure and location were plotted in Fig. 3, including their cycle-to-cycle variation. The effect of the C_1-C_3 percentage was more apparent at earlier SOI_{DIESEL}. M100 had a lower maximum in-cylinder pressure than other fuel blends but similar

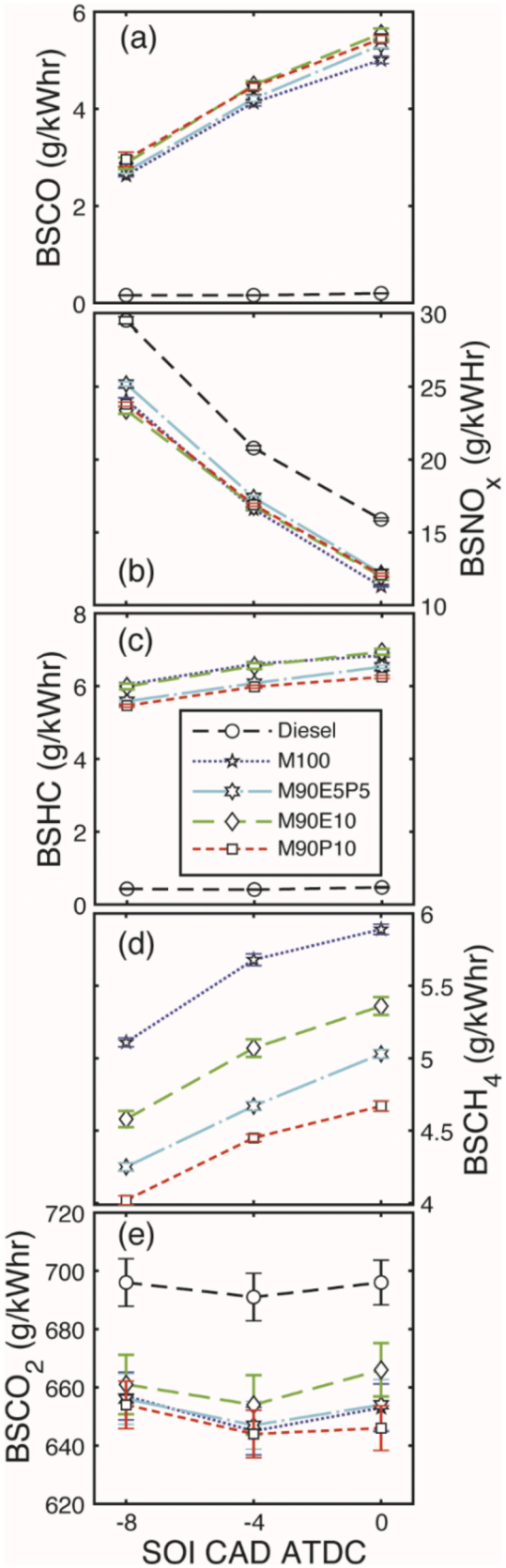

Fig. 6. Effect of C_1-C_3 composition on engine-out emissions at low-load dual-fuel operation. Error bars indicate the standard deviation of the measurement. Note: CH_4 exhaust emissions for diesel-only operation are not shown because they were negligible.

maximum pressure location to the other blends at $SOI_{DIESEL} = -4$ CA ATDC and TDC. The location of maximum pressure was the most repeatable for baseline diesel operation irrespective of the injection timing and least repeatable for M90P10 at SOI_{DIESEL} = TDC. Fig. 3 also suggests that improvement in the engine performance with M90P10 correlated with the higher maximum cylinder pressure and earlier location at $SOI_{DIESEL} = -8$ CA ATDC and -4 CA ATDC.

Apparent heat release rate (AHRR) plotted in Fig. 4 provides additional details about the effect of the C_1-C_3 percentage on combustion behavior. Previous work on the topic [27] suggests that the first AHRR peak seen in Fig. 4 was associated with the premixed combustion inside the bowl of the diesel fuel plus some of NG entrained inside the vaporized diesel. It started at local equivalence ratios closer to stoichiometry and continued in a leaning out mixture. As in-cylinder pressure and temperature increased, this premixed combustion extended inside the squish region, but at a slower rate, as turbulence decreased and the heat transfer to the wall increases, due to the higher surface-to-volume ratio in the squish region. The result was the second peak heat release rate seen in Fig. 4, which was also observed by the authors on previous work conducted on a single cylinder CI engine converted to SI operation that maintained the original diesel bowl-in-piston geometry [26]. As the equivalence ratio mentioned in Table 3 was very lean, Fig. 4 suggests that the combustion process after the first AHRR peak was a combination of flame propagation and autoignition, which was expected considering the high compression ratio (CR = 17) of this engine. This is where the change in the C_1-C_3 composition started to make a difference. It was more evident at advanced SOI_{DIESEL} due to the associated increase in bulk temperature (inferred from the higher in-cylinder pressure in Fig. 2), hence an increase in the kinetics rates. Specifically, Fig. 4 shows substantial differences in the second heat release peak location and magnitude. As expected, the mixtures with propane combusted faster inside the lower-turbulence and higher heat transfer squish region, due to propane's lower autoignition temperature. At the opposite, M100 had the lowest and most delayed second heat release peak. Therefore, it can be inferred that the autoignition temperature will play an important role in increasing or decreasing the combustion rate at low load operating conditions. Fig. 4 also shows that the differences between M90E5P5 and M90E10 were smaller than those between M90P10 and M90E5P5, probably due to larger differences in intake pressure and temperature than the other fuel blends. In addition, the differences in second AHRR peak at SOI_{DIESEL} = TDC were minimal, due to the increase in the squish volume at the time combustion reached that region compared to the more advanced SOI_{DIESEL} operation.

More information on the effect of the C_1-C_3 composition can be obtained by investigating changes in combustion phasing, which is known to affect thermal efficiency and emissions formation and oxidation. Fig. 5 shows CA50 (defined as the crank angle associated with 50% cumulative heat release), ignition delay (defined as the duration in CAD between SOI_{DIESEL} and the crank angle associated with 10% cumulative heat release), and the combustion duration (defined as the duration in CAD between the 10% and 90% cumulative heat release). Dual-fuel operation delayed CA50 at SOI_{DIESEL} of -4 CA ATDC and 0 CA ATDC (TDC). M100 produced the largest CA50 delay (~2 CAD), while the CA50 for M90E10, M90E5P5 and M90P10 being relatively similar. As CA50 in a diesel engine converted to spark ignition (SI) NG operation was near the end of the fast burn inside the piston bowl [27], it correlates with the small differences between M90E10, M90E5P5 and M90P10 first AHRR peak in Fig. 4. It is interesting to observe that CA50 for M90E10, M90E5P5 and M90P10 advanced slightly at $SOI_{DIESEL} = -8$CA ATDC. Fig. 5b suggests that this was due to the ignition delay becoming shorter as SOI_{DIESEL} advanced. Specifically, there was ~1 CAD increase in the ignition delay for M100 at SOI_{DIESEL} = TDC compared to a similar ignition delay to baseline diesel at $SOI_{DIESEL} = -8$ CA ATDC. This suggests that a relatively small change in SOI_{DIESEL} can have an important effect in the ignition delay of the dual-fuel operation, which is important from an engine control point of view. Specifically, engine

Table A1
Equipment used to measure most important experimental variables (type, make and model, and typical uncertainty).

Measured Parameter	Sensor Type	Sensor Manufacturer and Model	Range	Accuracy (+/-)	Uncertainty (max)
Engine Load	Load Cell	Lebow	1000 lb	0.25% full scale	2.5 lb
Engine Speed	Encoder	BEI XH25D-SS-1800	0–12,000 RPM 1800 bits/rev	0.06%	0.2 CAD
Methane Flow Rate	Flow Meter	AliCat MCP-100 SLPM	0–100 slpm	0.8% reading +/-0.2% full scale	1 slpm
Ethane Flow Rate	Flow Meter	AliCat MC-5 SLPM	0–5 slpm	0.8% reading +/-0.2% full scale	0.05 slpm
Propane Flow Rate	Flow Meter	AliCat MC-5 SLPM	0–5 slpm	0.8% reading +/-0.2% full scale	0.05 slpm
Diesel Mass per Data Point	Weight Scale	Brecknell MBS-6000	0–6000 g	0.02%	0.2 g
Intake Air Flow Rate	Laminar Flow Element (LFE)	Meriam 4-inch	0–400 SCFM	0.64% RDG	2.56 SCFM
LFE Air Pressure	Pressure Transducer	Omega PX277-05D5V	0–5 in. WC	1.00%	0.05 in. WC
Intake Air Pressure	High Speed Pressure Transducer	Kulite HEM-375-100A	0–100 PSIA	0.50%	0.5 PSIA
Exhaust Pressure	High Speed Pressure Transducer	Kulite EWCTV-312 M−100A	0–100 PSIA	0.50%	0.5 PSIA
Cylinder Pressure	High Speed Pressure Transducer	Kistler 6056A	0–250 bar	0.20%	0.5 bar

Table A2
Typical uncertainty for measured and calculated parameters, based on Eqns. (2)–(4).

Parameter	Typical error and unit
Diesel Mass Flow Rate	0.002 [g/s]
Gaseous Fuel Mass Flow Rate	0.006 [g/s]
Air Volumetric Flow Rate	0.26 [SCFM]
Global φ	0.012 [-]
Engine Torque	3.65 [ft-lb]
Engine Power	0.52 [kW]
BMEP	0.14 [bar]
Thermal Efficiency	0.84%
BSFC	4.7 [g/kW-hr]

manufacturers can update the original diesel operating map to allow for dual-fuel operation of a particular NG composition. As for the CA10-CA90 combustion duration, Fig. 5c suggests a similar decreasing trend with delayed SOI_{DIESEL} for all fuels. Dual-fuel operation with M100 increased the combustion duration by ~2–3 CAD, irrespective of the SOI_{DIESEL}. On the other hand, the combustion duration for M90E10, M90E5P5, and M90P10 was increased over the baseline diesel at all SOI_{DIESEL}, however was roughly half the increase experienced by M100. This is important because, at similar ignition delays as those in this work, a longer combustion duration can affect efficiency and emissions, as discussed next.

The differences in combustion phasing shown in Fig. 5 affected the performance data listed in Table 3. The 40% diesel replacement at these lower load dual-fuel operating conditions reduced BMEP by ~7%, which translated in ~3% lower brake efficiency. While the BMEP and brake thermal efficiency differences between the C_1-C_3 gas blends were relatively small, M90P10 consistently performed better while M100 produced the highest losses. However, the literature mentions that dual-fuel operation usually decreases engine performance, and the decrease in BMEP and thermal efficiency is similar to what was reported. The BSFC, COV of IMEP, and CO_2 emissions show that the decrease in engine performance this was not due to a decrease in engine combustion stability. The other important data in Fig. 6 are engine out emissions, because, as it was mentioned in the Introduction, it is important to minimize the aftertreatment requirements when switching to dual-fuel operation. The standard deviation for emissions is also shown. As expected, the change from diesel only to dual-fuel operation with port-fuel NG injection substantially increases CO and HC emissions, from 0.2 g/kWh and 0.4 g/kWh for diesel only operation to ~3 g/kWh and 6 g/kWh for dual-fuel operation, respectively. Most CO and HC emissions came from the NG trapped in chamber's crevices that, when re-entered into the combustion chamber during the expansion stroke, oxidized at lower pressure and temperatures. Among the gas blends, M90E5P5 and M90P10 had ~8% lower HC emissions compared to M100 and M90E10 cases, which correlates with the more advanced and higher second AHRR peak in Fig. 4 for blends with propane. The addition of propane also helped the most with the methane oxidation, as seen in Fig. 6 when CH_4 emissions are compared. Specifically, replacing 10% of C_1 with C_3 reduced CH_4 emissions by ~20% compared to a ~10% reduction when 10% of C_1 was replaced with C_2. It is important to mention that the reduction was similar at all SOI_{DIESEL}, which is an important observation from an engine-control point of view. This may also warrant the usage of higher C_3 fractions on diesel-NG dual-fuel combustion as C_2 has a higher demand for industrial processes (e.g., for plastics manufacturing). However, there was a different story for CO emissions. M90P10 had ~10% higher average CO emissions compared to M100, but M90P10 and M90E10 (i.e., the gas blends that showed the largest CO increase) had 3–4 times higher standard deviation, which makes it difficult to properly assess the fuel effect on CO emissions compared to the fuel effect on HC emissions. As for the NO_x emissions, the dual-fuel operation decreased them by ~20% on average. The decrease can be explained by the decrease in the local temperature, as the longer penetration of the diesel inside the combustion chamber in the dual-fuel operation created a leaner mixture at the start of combustion compared to diesel only operation. This is an important finding because it is more difficult to control NO_x than CO and HC emissions. Specifically, an oxidation catalyst can be added to treat the CO and HC emissions in a field application. As for the detailed effect of C_1-C_3 composition on NO_x emissions, the differences between fuels were larger at advanced SOI_{DIESEL}, when the gas autoignition temperature had a stronger influence on the local temperature.

4. Conclusions

This paper investigated the effect of natural gas (NG) composition on the efficiency and emissions of a dual-fuel diesel-NG engine operating at low load conditions. Part of the diesel fuel was replaced with four different gas blends containing methane (M), ethane (E) and propane (P) (M100, M90E10, M90E5P5, and M90E10; the numbers represent the volumetric percentage of the species in that gaseous mixture). In-cylinder pressure rise rate without EGR limited the diesel substitution rate. No EGR was employed to avoid it interfering with the evaluation of the effects of each individual fuel component. The total energy of the fuel (diesel or diesel plus gaseous fuel) was kept constant. NG was

injected inside the intake manifold just before the intake valve using low-pressure gas injectors. Three different diesel injection timings around the pure-diesel MBT timing were used. Therefore, the ignition process was like the one in a conventional diesel engine. The main conclusions were:

- BMEP for dual-fuel operation reduced compared to the diesel baseline, but the gas composition effect was limited. The 80% higher rates of pressure rise compared to the diesel baseline limited the low load dual-fuel diesel-NG engine operation at 40% substitution rate, irrespective of the injection timing.
- M100 had the longest diesel fuel vaporization and ignition delay with the most noticeable differences between individual NG compositions occurring during the late-stage fuel oxidation at early SOI_{DIESEL}. M100 had the largest increase in the ignition delay (~1 CAD at SOI_{DIESEL} = TDC), the largest CA50 delay (~2 CAD), and largest increase of combustion duration (2–3 CAD) compared to the baseline diesel, roughly double the increase experienced by the other gas mixtures. Specifically, the location and magnitude of the 2nd heat release peak changed with gas composition, with propane mixtures creating the most advanced location and the highest peak magnitude.
- In-cylinder pressure correlated with the gas mixture autoignition temperature (i.e., the order was M90P10 > M90E10 > M90E5P5 > M100). M90P10 generally had a higher maximum cylinder pressure and advanced location of maximum cylinder pressure compared to other fuels. As a result, the mixtures with propane had the best performance and gaseous fuel oxidation, while M100 had the worst. This would suggest maintaining a higher propane fraction and lower ethane fraction in the NG for dual-fuel operation.
- Dual-fuel operation reduced CO_2 and NO_x emissions up to 6.8% and 20%, respectively. However, it was offset by the large increase in CO and HC emissions, which could require after-treatment modifications.

The results suggests that the switch from diesel only to dual-fuel operation can be performed without major modifications in terms of engine control and aftertreatment changes, at least for the low load conditions and gas compositions used in this work.

Declaration of Competing Interest

The authors declare that they have no known competing financial interests or personal relationships that could have appeared to influence the work reported in this paper.

Acknowledgements

The material is based upon work funded by the WV Higher Education Policy Commission under grant number HEPC.dsr.18.7. The authors gratefully acknowledge WVU's Center for Innovation in Gas Research and Utilization (CIGRU) and the MAE department for their support (especially Kelsey Crawford and Derek Johnson). A special *thank you* to John Deere (Richard Winsor, Joseph Gonsowski, David Robinson, Bryan Geisick, Dou Danan, and many others) for providing the engine, engine components, and help with engine control. *Thank you* to VieleTech (Matt Viele and Kris Quillen) for providing support with DRIVVEN software and equipment. Finally, a special *thank you* to Jinlong Liu and Lorenzo Gasbarro for their contribution on the experimental setup during their time as graduate students at WVU.

Appendix A

Table A.1 shows the equipment used to measure the most important experimental variables in this work, including their associated uncertainty, as specified by the manufacturer.

Eq. (2) was used to calculate the standard deviation of all measured time-series parameters or the cycle-to-cycle variation for combustion parameters determined from in-cylinder pressure data:

$$\sigma = \sqrt{\frac{\sum (x_i - \mu)^2}{N}} \tag{2}$$

where σ is the standard deviation of the time-series measurement at a particular operating condition, x_i is an individual value in the time-series measurement, μ is the time-series measurement average, and N is the number of individual measurements in the time series data.

Eqs. (3) and (4) were used to determine the uncertainty for calculated parameters (e.g., engine power), using the general rules of error propagation:

$$q = f(x_1, x_2, \cdots, x_n) \tag{3}$$

$$\delta q = \sqrt{\left(\frac{\partial q}{\partial x_1}\delta x_1\right)^2 + \left(\frac{\partial q}{\partial x_2}\delta x_2\right)^2 \cdots \left(\frac{\partial q}{\partial x_n}\delta x_n\right)^2} \tag{4}$$

where q is the calculated parameter of interest (e.g., engine power), x_i are the variable used in the equation that calculates q, δq and δx_i are the uncertainties in the actual value of q and x_i, and $\partial q/\partial x_i$ is the partial derivative with respect to variable x_i of the function shown in Eq. (3).

Table A.2 shows the typical uncertainty for measured and calculated variables, based on the measurement errors in Table A.2 and Eqs. (2) to (4) above.

References

[1] Reuters, [Online]. Available: https://www.reuters.com/business/energy/us-heating-oil-diesel-stocks-dwindle-demand-rises-2022-02-04/. [Accessed 12 February 2022].
[2] "How much carbon dioxide is produced when different fuels are burned?," U.S. Energy Information Administration, 8 October 2021. [Online]. Available: https://www.eia.gov/tools/faqs/faq.php?id=73&t=11. [Accessed 12 February 2022].
[3] M. Foss, J. Wardzinski and F. Delano, "Interstate Natural Gas – Quality Specifications & Interchangeability," Center for Energy Economics, Austin Texas, 2004. [Online] Available: https://www.beg.utexas.edu/files/energyecon/global-gas-andlng/. CEE_Interstate_Natural_Gas_Quality_Specifications_and_Interchangeability.pdf. [Accessed 12 February 2022].
[4] Omnitek, "Diesel-to-Natural Gas Engine Conversions," [Online]. Available: https://www.omnitekcorp.com/images/Diesel-to-Natural%20Gas%20Engine%20Conversions.pdf. [Accessed 11 Janurary 2022].
[5] Gasbarro L, Liu J, Dumitrescu C, Ulishney C, Battistoni M, Ambrogi L. Heavy-Duty Compression-Ignition Engines Retrofitted to Spark-Ignition Operation Fueled with

Natural Gas. SAE Technical Paper 2019–24-0030, 2019.. https://doi.org/10.4271/2019-24-0030.
[6] "Dual Fuel Conversions," Penn Power Group, [Online]. Available: https://pennpowergroup.com/solutions/dual-fuel-conversions/. [Accessed 11 January 2022].
[7] Law CK. Combustion Physics. New York: Cambridge University Press; 2006.
[8] "Fuels – Higher and Lower Calorific Values," The Engineering Toolbox, 2003. [Online]. Available: https://www.engineeringtoolbox.com/fuels-higher-calorific-values-d_169.html. [Accessed 11 January 2022].
[9] Ambrogi L, Liu J, Battistoni M, Dumitrescu C, Gasbarro L. CFD Investigation of the Effects of Gas' Methane Number on the Performance of a Heavy-Duty Natural-Gas Spark-Ignition Engine. SAE Technical Paper 2019–24-0008, 2019.. https://doi.org/10.4271/2019-24-0008.
[10] Engineering ToolBox. "Fuels and Chemicals- Autoignition Temperatures." 2003. [Online]. [Accessed 8 January 2022].
[11] Yang X, Vinhaes V, Turcios M, Huang J, Naber J. Process for Study of Micro-pilot Diesel-NG Dual Fuel Combustion in a Constant Volume Combustion Vessel Utilizing the Pre-mixed Pre-burn Procedure. SAE Technical Paper 2019–01-1160, 2019.. https://doi.org/10.4271/2019-01-1160.
[12] Garcia P, Tunestal P. Experimental Investigation on CNG-Diesel Combustion Modes under Highly Diluted Conditions on a Light-Duty Diesel Engine with Focus on Injection Strategy. SAE Technical Paper 2015;8(5):2177–87.
[13] Muralidharan M, Srivastava A, Subramanian M. A Technical Review on Performance and Emissions of Compressed Natural Gas-Diesel Dual Fuel Engine. SAE Technical Paper 2019–28-2390, 2019..
[14] Zhang B, Mazlan S, Jiang S, Boretti A. Numerical Investigation of Dual Fuel Diesel-CHG Combustion on Engine Performance and Emissions. SAE Technical Paper 2015–01-0009, 2015.. https://doi.org/10.4271/2015-01-0009.
[15] Li Y, Guo H, Li H. Evaluation of Kinetic Process in CFD Model and Its Application in Ignition Process Analysis of a Natural Gas-Diesel Dual Fuel Engine. SAE Technical Paper 2017–01-0554, 2017.. https://doi.org/10.4271/2017-01-0554.
[16] Cameretti M, Robbio R, Tuccillo R. Performance Improvement and Emission Control of a Dual Fuel Operated Diesel Engine. SAE Technical Paper 2017–24-0066, 2017.. https://doi.org/10.4271/2017-24-0066.
[17] Guido C, Napolitano P, Fraioli V, Beatrice C, Giacomo ND. Assessment of Engine Control Parameters Effect to Minimize GHG Emissions in a Dual Fuel NG/Diesel Light Duty Engine. SAE Technical Paper 2018–01-0266, 2018.. https://doi.org/10.4271/2018-01-0266.
[18] Robbio R, Cameretti M, Mancaruso E, Tuccillo R, Vaglieco B. Combined CFD-Experimental Analysis of the In-Cylinder Combustion Phenomena in a Dual-Fuel Optical Compression Ignition Engine. SAE Technical Paper 2021–24-0012, 2021.. https://doi.org/10.4271/2021-24-0012.
[19] Zhu Z, Li Y, Shi C. Effects of natural gas energy fractions on combustion performance and emission characteristics in an optical CI engine fueled with natural gas/diesel dual-fuel. Fuel 2022;307(1):121842. https://doi.org/10.1016/j.fuel.2021.121842.
[20] You J, Liu Z, Wang Z, Wang D, Xu Y, Du G, et al. The exhausted gas recirculation improved brake thermal efficency and combustion characteristics under different intake throttling conditions of a diesel/natural gas dual fuel engine at low loads. Fuel 2020;266(1):17035. https://doi.org/10.1016/j.fuel.2020.117035.
[21] Wang Z, Zhao Z, Wang D, Tan M, Han Y, Liu Z, et al. Impact of pilot diesel ignition mode on combustion and emissions characteristcs of a diesel/natural gas dual fuel heavy-duty engine. Fuel 2016;67(1):248–56.
[22] G. Smith, D. Golden, M. Frenklach, N. Moriarty, B. Eiteneer, M. Goldenberg, T. Bowman and R. Hanson, "GRI-Mech 3.0," Berkeley, [Online]. Available: http://combustion.berkeley.edu/gri-mech/version30/text30.html#cite. [Accessed 8 January 2022].
[23] "Wartsila Methane Number Calculator," Wartsila, 2022. [Online]. Available: https://www.wartsila.com/marine/products/gas-solutions/methane-number-calculator. [Accessed 8 January 2022].
[24] Hall C, Kassa M. Advances in combustion control for natural gas-diesel dual fuel compression ignition engines in automotive applications: A review. Renew Sustain Energy Rev 2021;148(1):111291. https://doi.org/10.1016/j.rser.2021.111291.
[25] J. Liu and C. Dumitrescu, "Lean-Burn Characteristcs of a Heavy-Duty Diesel Engine Retrofitted to Natural-Gas Spark Ignition," *J. Eng Gas Turbines Power* 141(7), p.071013, 2019. doi.10.1115/1.4042501.
[26] C. Ulishney, J. Liu, C. Dumitrescu and A. Sivri, "Effect of Bowl-In-Piston Chamber on the Combustion Process in a Stoichiometric Natural-Gas Spark-Ignition Engine," in *International Conference on Applied Energy*, Aug 12-16, 2019, Vasteras, Sweeden, Paper 343, 2019.
[27] J. Liu, C. Ulishney and C. Dumitrescu, "Characterizing Two-Stage Combustion Process in a Natural Gas Spark Ignition Engine Based on Mulit-Weibe Function Model," *Journal of Energy Resources Technology* 142(10), p. 102302, 2020. doi.10.1115/1.4046793.